Intelligent Equipment and Special Robots
Q. Zhang (Ed.)

doi:10.3233/ATDE240220

Design of the Slave Hand Structure and Interference Detection for the Master-Slave Craniotomy Surgical Robot

Lei ZHAO[a,b], Guobin ZHANG[a,b], Zehua LI[a,b] and Zhenzhong LIU[a,b1]
[a] *Tianjin Key Laboratory for Advanced Mechatronic System Design and Intelligent Control, School of Mechanical Engineering, Tianjin University of Technology, Tianjin 300384, China*
[b] *National Demonstration Center for Experimental Mechanical and Electrical Engineering Education (Tianjin University of Technology), Tianjin, China*

Abstract. Existing neurosurgical robots are prone to interfering with each other in a narrow operating space due to the overlapping of several arms, which poses a great safety risk during surgery. In this paper, a 7-DOF dual-arm robot is designed to cooperate with the surgeon to complete craniotomy by manipulating the master hand mechanism. Aiming at the pain point that two real-time dynamic slave hands are prone to interference, this paper establishes a simplified model of the robot envelope, and transforms the interference detection problem between the robots into the interference checking of geometric primitives. If the interference between the two arms is detected by the algorithm, the surgical path of the current robotic arm is immediately terminated to ensure the safety of the surgery. Finally, the algorithm is simulated and verified with the robot designed in this paper. The results show that the algorithm is feasible and has high computational efficiency.

Keywords. Surgical robot, structural design, enclosing box, interference detection

1. Introduction

The master-slave surgical robot is an important achievement in the development of medical robotics, which combines the high precision and stability of robotic technology with the surgeon's clinical experience, greatly improving the efficiency of surgery while reducing the surgeon's surgical burden[1,2]. In recent decades, the development of endoscopy, surgical navigation, neuroimaging, neuromodulation and other technologies has played an important role in promoting the development of the field of neurosurgery. Especially after the NeuroMate robot was certified by the U.S. FDA[3], neurosurgical surgical robots have been developed at a high speed, and many representative neurosurgical surgical robots have been developed at home and abroad. The University of Calgary in Canada developed NeuroArm, the world's first dedicated surgical robotic system for neurosurgical intracranial operations[4]. The ROSA One Brain[5] developed by Zimmer Biomet, USA, utilizes sensing technology, haptic feedback, and dynamic

[1] Corresponding Author: Zhenzhong LIU, Tianjin Key Laboratory for Advanced Mechatronic System Design and Intelligent Control; National Demonstration Center for Experimental Mechanical and Electrical Engineering Education; Tianjin University of Technology; e-mail: 15904525440@163.com

tracking technology and was approved by the FDA for neurosurgery in 2019. There are also surgical robots such as CARNIO from RWTH Aachen University in Germany and CASPAR from Heidelberg University. Domestic neurosurgical robots are mainly used in stereotactic surgery. For example, the Remebot surgical robot developed by Parkwell Wellcome[6] and CARS, a robotic system jointly developed by the Naval General Hospital and Beijing University of Aeronautics and Astronautics. Considering the narrow operating space for craniotomy surgery, several dynamic surgical robotic arms are prone to produce interference phenomenon during surgical operation and other factors, the robot that can complete craniotomy surgery has not been clinically applied in the medical system[7]. Thus, effective and accurate interference detection is one of the prerequisites for the safe and stable operation of surgical robotic systems.

At present, interference detection can be categorized into two detection methods: sensing and building mode. Sensor-based interference detection utilizes external sensor devices to complete real-time detection, which not only increases the complexity of the system but also is constrained by environmental factors[8]. The modeling interference detection is to judge the interference situation by the positional relationship of the established model, which is easy to realize and can reduce the cost, so this method is mostly used in practical applications[9,10]. The method of simplifying the joints and connecting rods of the robotic arm into a number of spheres only needs to calculate the distance between the centers of the spheres, which is a small amount of computation, but it will produce a large amount of invalid space and poor accuracy. Modeling using axis-aligned bracket box (AABB) and orientation bracket box (OBB)[11], the model has low fit and poor detection accuracy. Modeling using triangular face sheets, the model accuracy is high, but the hardware requirements are high and the detection efficiency is low, which is not suitable for security detection. The modeling with capsule enclosing box and sphere enclosing box simplifies the calculation on the basis of guaranteeing accuracy, but it is only applicable to some robot models. In order to avoid the drawbacks of other modeling methods and fit the actual robot model, this paper adopts two geometric primitives, cylinder and sphere, to envelope the robotic arm for real-time interference detection.

2. Structural design of the slave hand

Craniotomy robots usually need at least six degrees of freedom to realize rotation and translation in three-dimensional space. To better reproduce the operation of the doctor's main hand end and realize the precise positioning and operation of the target area, this paper refers to the arm part of the human body from the hand in the configuration of the degrees of freedom, and each of the two robotic arms has been designed with seven rotational degrees of freedom, so as to make it have a movement ability closer to the human arm and have a high degree of flexibility.

As shown in Figure 1, the robot base is fixedly mounted on the ground to avoid as much as possible the vibration in the environment affecting the accuracy of the robot. The height of the base is 1300mm, so that the working space of the robotic arm covers the operating area of the operating table with a standard height of 600-950mm. The mounting surface of the two robotic arms is 90 degrees perpendicular to the space, which can reduce the problem of interference between the two robotic arms to a certain extent while further expanding the total working space of the two robotic arms. Each joint adopts modularized supple joints, integrating various components such as drive motors, speed reducers, loss-of-electricity brakes, sensors, etc., which significantly reduces the structural complexity of the robotic arm and at the same time meets the high-precision requirements of the robotic arm.

The robotic arm part of the surgical robot uses aluminum alloy or carbon fiber composite materials. The use of these materials has good strength and rigidity, while the weight is relatively light, to avoid surgical errors due to the inertia of the robotic arm, affecting the accuracy of surgical operations. The joints and connecting parts of the robotic arm are made of titanium alloy and stainless steel high-strength metal alloy, which has excellent corrosion resistance and mechanical properties to ensure the stability and reliability of the robotic arm. The surgical execution tools at the end of the robot are made of stainless steel. Stainless steel is biocompatible, easy to sterilize and corrosion-resistant, while being able to withstand the stresses of surgical operations.

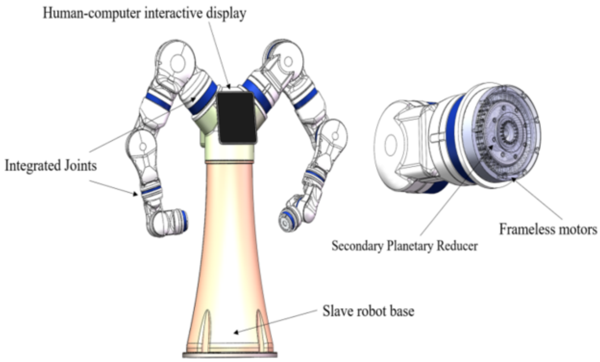

Figure 1. 3D model of the slave hand

3. Interference detection analysis

3.1. Simplified model of a double robotic arm

Considering that the robotic arm is composed of complex and irregular metal parts, the efficiency of detection is improved by enveloping and simplifying it with an enveloping box. As shown in Figure 2, it is one of the geometrical models of robotic arm envelope simplification, including three cylinders and three spheres, the joints and connecting rods of the robotic arm are embedded in the geometrical model, and the dimensional parameters of the cylinders and spheres are shown in Table 1.

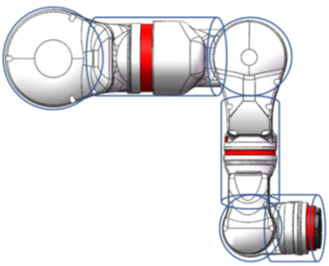

Figure 2. Simplified model of robot arm enclosing box.

Table 1. Parameter list of enclosing box dimensions

Geometric modulus	J_1	J_2	J_3	L_1	L_2	L_3
Radius/mm	124	88	65	92	85	62
Lengths/mm				380	365	120

3.2. Interference detection algorithm

According to the simplified model of the robot, the interference of the two robotic arms can be transformed into the calculation of the distance between the various geometric units of these two simplified models. When the shortest distance between any two geometric primitives is equal to 0, it means that the two produce an interference phenomenon. This can be refined into three types of calculations: the distance between the sphere and the sphere, the distance between the sphere and the cylinder, and the distance between the cylinder and the cylinder. The following three forms of interference are judged.

3.2.1. Interference judgment of sphere to sphere

From the positive kinematics of the robot, the coordinates of the spherical centers of the spherical enclosing boxes with two joints at the end and the coordinates of the two endpoints of the central line segment of the cylindrical enclosing boxes can be calculated. Assuming that the spherical coordinates of the two spherical centers are $O_A(x_A, y_A, z_A)$ and $O_B(x_B, y_B, z_B)$, and the radius are r_{OA} and r_{OB}, the Euclidean distance between the two spherical centers can be obtained as Eq. (1).

$$d_{ss} = \sqrt{(x_B - x_A)^2 + (y_B - y_A)^2 + (z_B - z_A)^2} \tag{1}$$

In turn, the shortest distance between the two spheres is $L_{ss} = d_{ss} - r_{OA} - r_{OB}$. If $L_{ss} > 0$, then it is shown that the two do not interfere.

3.2.2. Interference judgment of sphere and cylinder

The distance between the sphere and the cylinder can be simplified as the center of the sphere to the cylinder within the shortest distance from the center line. Suppose the coordinates of the center of the sphere is $P(x_0, y_0, z_0)$, and the radius of the sphere is r_0. The two endpoints of the center line segment inside the cylinder are $C(x_c, y_c, z_c)$ and $D(x_d, y_d, z_d)$, and the radius of the cylinder is r_{cd}. Through the point *P* to the straight line *CD* as a vertical line and the straight line *CD* intersects the point *M*, it is easy to know the location of the point *M* there are three cases: point *M* on the left side of the point *C*; point *M* on the line *CD*; point *M* on the right side of the point *D*, the three cases shown in Figure 3.

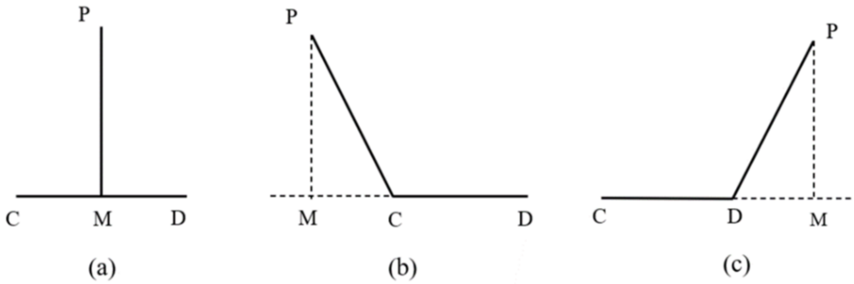

Figure 3. Three relationships between points and line segments.

Define $\overrightarrow{CM}$ as $\overrightarrow{CP}$ the vector of projections on the line CD, then $CM = \frac{(CP \cdot CD)}{|CD|^2} AB$. Let $t = \frac{(CP \cdot CD)}{|CD|^2}$,determine the relationship between the point *M* and the relative position of the line *CD* by the range of values of *t*. If 0<*t*<1, then the point *M* is on the line *AB*, as shown in (a), then the shortest distance is $|PM|$. When $t \le 0$ and $t \ge 0$, respectively, represent the two cases of (b) and (c) in the figure 3, the shortest distance is $|PC|$ and $|PD|$, respectively, using the Eq. (1).can be found. Regarding the solution of $|PM|$, in this paper, the triangular equal area method is used to solve the$|PM|$, We get $|PM| = \frac{|PC \times PD|}{|CD|}$. In summary, the distance from the center of the sphere to the center line segment of the cylinder is

$$d_{sc} = \begin{cases} \mathrm{d}_{PC} = \sqrt{(x_c - x_0)^2 + (y_c - y_0)^2 + (z_c - z_0)^2}, t \le 0 \\ \mathrm{d}_{PM} = \frac{|PC \times PD|}{|CD|}, 0 < t < 1 \\ \mathrm{d}_{PD} = \sqrt{(x_d - x_0)^2 + (y_d - y_0)^2 + (z_d - z_0)^2}, t \ge 1 \end{cases} \tag{2}$$

Then the shortest distance between the sphere and the cylinder $L_{sc} = d_{sc} - r_o - r_{cd}$ .If $L_{sc} > 0$, then there will be no interference between the sphere and the cylinder.

3.2.3. Determination of interference between a cylinder and a cylinder

The cylinder-to-cylinder interference is more complicated in the interference model with two robotic arms. Assume that the central line segments L_1 and L_2 of two cylinders in space:

$$\begin{cases} L_1: M(\lambda_1) = M_0 + \lambda_1(M_1 - M_0) = M_0 + \lambda_1 u \quad , 0 \le \lambda_1 \le 1 \\ L_2: N(\lambda_2) = N_0 + \lambda_2(N_1 - N_0) = N_0 + \lambda_2 v \quad , 0 \le \lambda_2 \le 1 \end{cases} \tag{3}$$

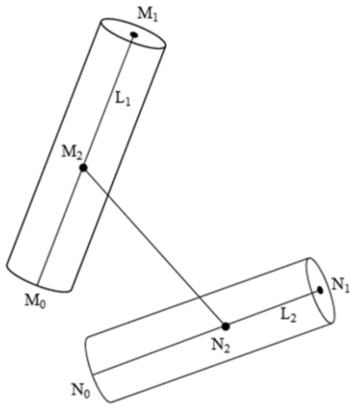

Figure 4. Cylindrical enclosing box model.

As shown in Figure 4, M_0 and M_1 are the two endpoints of line L_1, and N_0 and N_1 are the two endpoints of line L_2, respectively. Where λ_1 and λ_2 are two scale factors. $\vec{u}$ and $\vec{v}$ are two direction vectors, $\vec{u} = M_1 - M_0$, $\vec{v} = N_1 - N_0$. The mathematical model to calculate the shortest distance between the central line segments of two cylinders is

$$\min d(\lambda_1, \lambda_2) = \|M(\lambda_1) - N(\lambda_2)\|^2 = \|(M_0 + \lambda_1 u) - (N_0 + \lambda_2 v)\|^2 \tag{4}$$

According to the minimal value condition: let $\frac{\partial d}{\partial \lambda_1} = 0$, $\frac{\partial d}{\partial \lambda_2} = 0$, so that the values of the scale factors λ_1, λ_2 can be determined:

$$\begin{cases} \lambda_1 = \dfrac{(u \cdot v)\left[(M_0 - N_0) \cdot v\right] - \|v\|^2 \left[(M_0 - N_0) \cdot u\right]}{\|u\|^2 \|v\|^2 - (u \cdot v)^2} \\ \\ \lambda_2 = \dfrac{(u \cdot v)\left[(M_0 - N_0) \cdot u\right] - \|u\|^2 \left[(M_0 - N_0) \cdot v\right]}{\|u\|^2 \|v\|^2 - (u \cdot v)^2} \end{cases} \tag{5}$$

Let M_2 and N_2 be the two vertical feet of the central segment of the cylinders M_0M_1 and N_0N_1, and let r_1 and r_2 be the radius of the two cylinders respectively. Then M_2 has three possibilities for M_0M_1: (1) when M_2 is on the reverse extension of M_0M_1.(2) when M_2 is on the line segment M_0M_1. (3) when M_3 is on the extension of M_1M_2. Similarly, it can be seen that N_2 is equivalent to N_0N_1 there are also three cases. So a total of 9 cases can be obtained by combining the two. When $0 \le \lambda_1 \le 1$ and when $0 \le \lambda_2 \le 1$, it can be deduced that the foot of the common vertical line of L_1 and L_2 falls exactly within the two line segments, the shortest distance $d_{cc} = \|M_2N_2\| = \sqrt{d(\lambda_1, \lambda_2)}$ at this time. The shortest distance in all cases is shown in Eq. (6):

$$d_{cc} = \begin{cases} \|M_0N_0\| & \lambda_1 < 0, \lambda_2 < 0 \\ \|M_0N_2\| & \lambda_1 < 0, 0 \le \lambda_2 \le 1 \\ \|M_0N_1\| & \lambda_1 < 0, \lambda_2 > 1 \\ \|M_2N_0\| & 0 \le \lambda_1 \le 1, \lambda_2 < 0 \\ \|M_2N_2\| & 0 \le \lambda_1 \le 1, 0 \le \lambda_2 \le 1 \\ \|M_2N_1\| & 0 \le \lambda_1 \le 1, \lambda_2 > 1 \\ \|M_1N_0\| & \lambda_1 > 1, \lambda_2 < 0 \\ \|M_1N_2\| & \lambda_1 > 1, 0 \le \lambda_2 \le 1 \\ \|M_1N_1\| & \lambda_1 > 1, \lambda_2 > 1 \end{cases} \tag{6}$$

Then the shortest distance between the cylinder and the other cylinder is $L_{cc} = d_{cc} - r_1 - r_2$, If $L_{cc} > 0$, then there is no interference between the two cylinders.

4. Robot simulation experiment

In order to verify the feasibility of this algorithm, the robot designed in this paper is taken as the research object and the simulation model of the initial pose of the robot is built in MATLAB as shown in Figure 5. The distance between the interference detection envelope boxes is calculated in full alignment, from which the minimum value is selected as the shortest distance between the two arms. The shortest distance between the two robotic arms at the initial moment is 630 mm, and its D-H parameters are derived according to the dimensions of the robot as shown in Table 2. In this paper, it is planned that the two robotic arms from the hand end approach each other slowly and must collide at the end point to verify the accuracy of the interference detection model.

Table 2. D-H parameter table of the robot

i	α /°	a/mm	d/mm	θ /°
1	-90	0	293	θ_1
2	90	0	0	θ_2
3	-90	0	490	θ_3
4	90	0	0	θ_4
5	-90	0	422	θ_5
6	90	0	0	θ_6
7	0	0	175	θ_7

According to the interference detection algorithm introduced above for the dual robotic arms in the displacement state corresponding to each motion moment, the shortest distance between the dual robotic arms can be obtained at all moments during the process from the starting point to the end point. The red line in Figure 5 is the connecting line of the shortest position of the distance between the two robotic arms in this state as determined by the algorithm. Figure 6 shows the position and attitude of the two mechanical arms at the end of the two movements. Figure 7 represents the arc change of the seven joints over time during the whole movement.

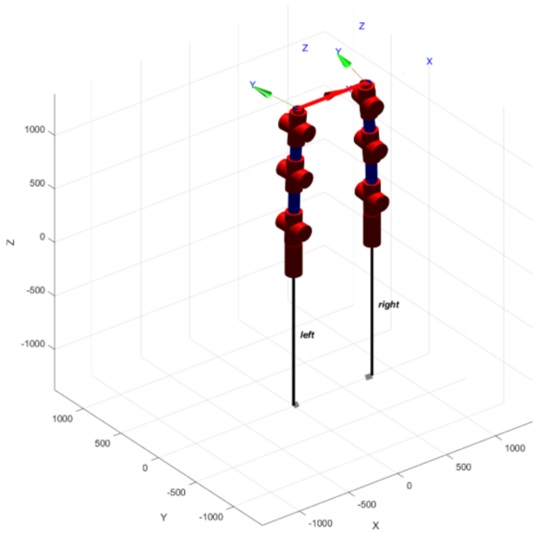

Figure 5. Position and attitude of the robot at the initial moment.

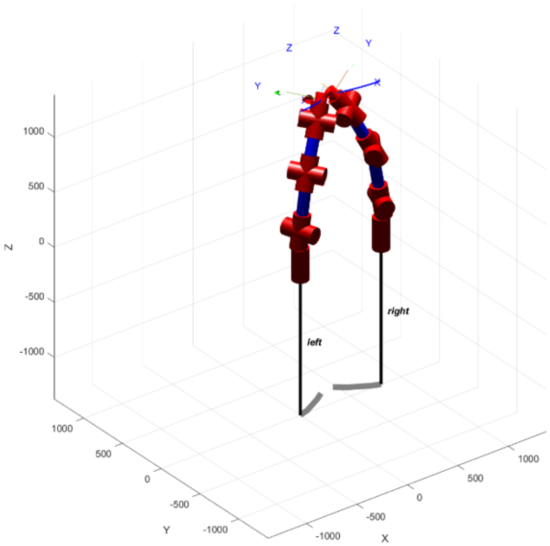

Figure 6. Position and attitude of the robot at the end moment.

The shortest distance between the two robotic arms is shown in Fig. 8, and it can be judged that the distance between the robots reaches 0 at about 42 seconds. From this, it can be seen that the two robotic arms are about to interfere at 42 seconds. The two robotic arms are about to interfere with each other. After detecting the impending interference, the two robotic arms are made to stop the current movement path immediately, so as to avoid the collision of the two robotic arms as they continue to move.

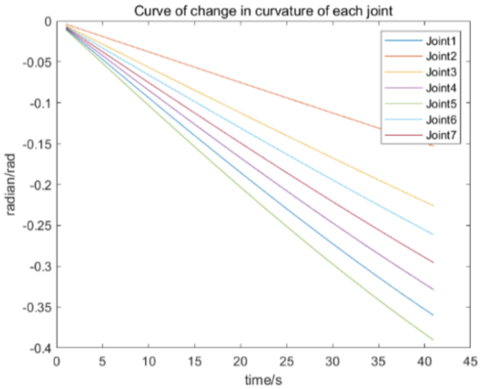

Figure 7. Curve of change in curvature of each joint.

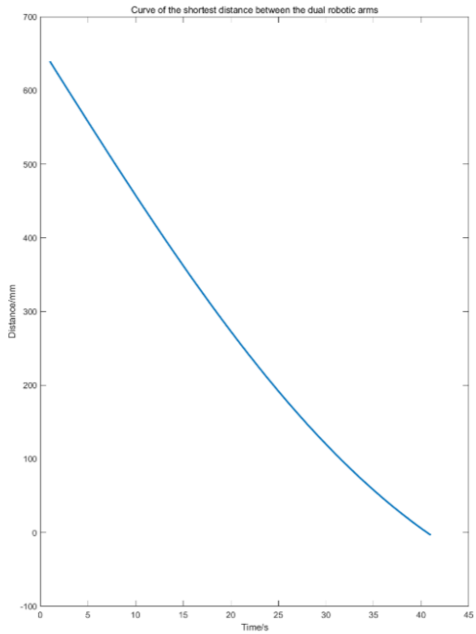

Figure 8. Curve of the shortest distance between the dual robotic arms

5. Conclusion

In this paper, for the phenomenon that two robotic arms are prone to interfering with each other in the process of following the movement of the master hand, two geometric primitives, cylinder and sphere, are used to simplify the envelope of the robotic arms, and the real-time distance between the geometric primitives is computed to determine whether or not the interference occurs between the robotic arms. The distances from points to line segments are calculated using vector and geometric methods, and for line segment to line segment distances are discussed in separate cases. If the algorithm calculates an interference between the arms, the current motion of the robot is stopped immediately, which guarantees the safety of the surgical process. The algorithm is versatile, without additional computer equipment and complex operating environment, reducing the application cost. And the algorithm can dynamically change the radius of the enclosing box model according to the actual running speed of the robotic arm, which can ensure that the robot can complete the surgical task, but also leave processing space for the robotic arm to avoid obstacles or braking. The algorithm is applied to the robot designed in this paper, and simulation verification is carried out in MATLAB by detecting the shortest distance between the two arms in real time. The simulation results show the effectiveness of the algorithm.

References

[1] Wu.Zhang, Li.Haiyuan, Cui.Linlin, Li.Haiyang, Zhang.Xiangyan, Fang.Shanxiang, Zhang.Qinjian, Research progress and development trend of surgical robot and surgical instrument arm, *The International Journal of Medical Robotics and Computer Assisted Surgery* **17** (2021), e2309.

[2] Saroha.Abhimanyu, Gupta.Neha. Revolutionizing Surgery: A Review of the Advancements and Challenges in AI and Robotic Surgery, *2023 International Conference on Sustainable Computing and Smart Systems (ICSCSS). IEEE* （2023）， 515-523.

[3] Langsdorff.Daniel.von, Paquis.Philippe, Fontaine.Denys, In vivo measurement of the frame-based application accuracy of the Neuromate neurosurgical robot, *Journal of neurosurgery* **122** (2015), 191-194.

[4] Sutherland.Garnette.R, Lama.Sanju, Gan.Liu.Shi, Wolfsberger.Stefan, Zareinia.Kourosh, Merging machines with microsurgery: clinical experience with neuroArm, *Journal of neurosurgery* **118** (2013), 521-529.

[5] Tran.Diem.Kieu, Paff.Michelle, Mnatsakanyan.Lilit, Sen-Gupta.Indranil, Lin.Jack.J, Hsu.Frank.P.K, Vadera.Sumeet, A novel robotic-assisted technique to implant the responsive neurostimulation system, *Operative Neurosurgery* **18** (2020), 728-735.

[6] Wang.Tao, Zhao.Quan-Jun, Gu.Jian-Wen, Shi.Tie-Jun, Yuan.Xujun, Wang.Jia, Cui.Shao-Jie, Neurosurgery medical robot Remebot for the treatment of 17 patients with hypertensive intracerebral hemorrhage, *The international journal of medical robotics and computer assisted surgery* **15** (2019), e2024.

[7] Elsabeh.Rami, Singh.Sukhbir, Shasho.Jeff, Saltzman.Yoni, Abrahams.John.M, Cranial neurosurgical robotics, *British journal of neurosurgery* **35** (2021), 532-540.

[8] Ji.Sungho, Shin.Jaehee, Yoon.Jiyoung, Lim.Kwang-Hyeok, Sim.Gi-Dong, Lee.Yong-Seok, Kim.Duck.Hwan, Cho.Hanchul, Park. Jinhyoung, Three-dimensional skin-type triboelectric nanogenerator for detection of two-axis robotic-arm collision, *Nano Energy* **97** (2022), 107225.

[9] Cieślak.Patryk, Simoni.Roberto, Rodríguez.Pere.Ridao, Youakim.Dina, Practical formulation of obstacle avoidance in the Task-Priority framework for use in robotic inspection and intervention scenarios, *Robotics and Autonomous Systems* **124** (2020), 103396.

[10] Wang.Xuewu, Yan.Yixin, Gu.Xingsheng, Spot welding robot path planning using intelligent algorithm, *Journal of Manufacturing Processes* **42** (2019), 1-10.

[11] Jasim.Ali, Qi.TangXiao, Bao.Song, Collision detection and trajectory planning for palletizing robots based OBB, *Indonesian Journal of Electrical Engineering and Computer Science* **1** (2016), 109-118.